Acta Materialia 206 (2021) 116610

Contents lists available at ScienceDirect

Acta Materialia

journal homepage: www.elsevier.com/locate/actamat

Design and development of high-power piezoelectric ceramics through integration of crystallographic texturing and acceptor-doping

Haoyang Leng[a], Yongke Yan[a,*], Hairui Liu[a], Mark Fanton[b], Richard J. Meyer[b], Shashank Priya[a,*]

[a] Department of Materials Science and Engineering, The Pennsylvania State University, University Park, Pennsylvania 16802, United States
[b] Applied Research Laboratory, The Pennsylvania State University, University Park, PA, 16801, USA

ARTICLE INFO

Article history:
Received 7 August 2020
Revised 22 December 2020
Accepted 25 December 2020
Available online 30 December 2020

Keywords:
Texturing
Acceptor
Doping
Piezoelectric
Ceramics
Transducer

ABSTRACT

This study demonstrates the integrated approach based upon texturing and acceptor doping for realizing a high-power piezoelectric ceramic with combined soft and hard properties. The textured Mn-doped 0.24 $Pb(In_{1/2}Nb_{1/2})O_3$-0.42 $Pb(Mg_{1/3}Nb_{2/3})O_3$-0.34 $PbTiO_3$ (PIN-PMN-PT) ceramic exhibits enhanced piezoelectric coefficient d_{33} and electromechanical coupling factor k_{31} in comparison with random counterpart. This enhanced piezoelectric response originates from the combined intrinsic high piezoelectric properties of <001>-oriented grains, and reduced energy barrier for polarization rotation in textured ceramics. The $BaTiO_3$ (BT) template in textured ceramics increases the tetragonality degree which results in improved coercive field E_c but decreased mechanical quality factor Q_m in comparison with random counterpart. The decreased Q_m values of textured ceramics are related to the crystallographic dependence of Q_m and the enhanced domain mobility due to the existence of small size domains. The textured ceramic with 2 vol.% BT content exhibited an excellent combination of soft and hard piezoelectric properties, measured to be: d_{33} = 517 pC/N, Q_m = 1147, E_c = 10.0 kV/cm, and tan δ = 0.49%, which is highly promising for high power piezoelectric applications.

1. Introduction

Piezoelectric materials are widely used in underwater transducers, actuators, motors, and transformers due to the inherent coupling between the electrical and mechanical signals. [1–4] Piezoelectrics used in high power applications require high vibration velocity v_{rms} in order to generate high mechanical power. [5–7] In order to obtain a high vibration velocity ($v_{rms} \propto Q_m \cdot d$), piezoelectric materials should possess high mechanical quality factor (Q_m) and piezoelectric strain coefficient (d). Further, when devices are subjected to high electric fields; high coercive fields (E_c), low dielectric/mechanical losses (tan δ), and high electromechanical coupling coefficient (k) is necessary for effective electrical to mechanical energy conversion. Thus, high power piezoelectric materials should possess both soft and hard properties at the same time in order to meet these requirements.

The design and synthesis of high-power piezoelectric ceramics is challenging since the hard properties (high Q_m and low tan δ) are caused by the "pinned" ferroelectric domain state through acceptor doping, [5,8–10] which will degrade the soft properties (high d_{33} and high k). [6,11] Thus, most of the state-of-the-art acceptor-doped piezoelectric ceramics exhibit non-optimum combination of soft and hard properties as shown in Fig. 1. [8,12] Piezoelectric single crystals exhibit excellent soft properties but have low coercive field (E_c), low mechanical toughness, and relatively high cost of production. [13–15] Texturing technique has been developed to achieve grain-oriented piezoelectric ceramics with low-cost in comparison with single crystals, reasonable piezoelectric properties but high mechanical strength and rate of production. [16–18] One of the methods to fabricate textured piezoelectric ceramics is templated grain growth (TGG). [19–22] We demonstrate that high power piezoelectrics can be designed by integration of texturing method (to enhance "soft" characteristics) and acceptor doping (to enhance "hard" characteristics).

Recently, <001> textured PMnS-PMN-PZT ceramics with a texturing degree of 50% have been reported to exhibit a moderate combination of d_{33} (445 pC/N) and Q_m (824), [23] but their relatively low coercive field (E_c of 8 kV/cm) still restricts their applications in high power field, indicating that both compositional and processing modifications are required to enhance texturing degree and high-power properties. Relaxor-based $Pb(In_{1/2}Nb_{1/2})O_3$-$Pb(Mg_{1/3}Nb_{2/3})O_3$-$PbTiO_3$ (PIN-PMN-PT) ternary ferroelectrics have

* Corresponding authors.
E-mail addresses: yxy355@psu.edu (Y. Yan), sup103@psu.edu (S. Priya).

https://doi.org/10.1016/j.actamat.2020.116610
1359-6454/

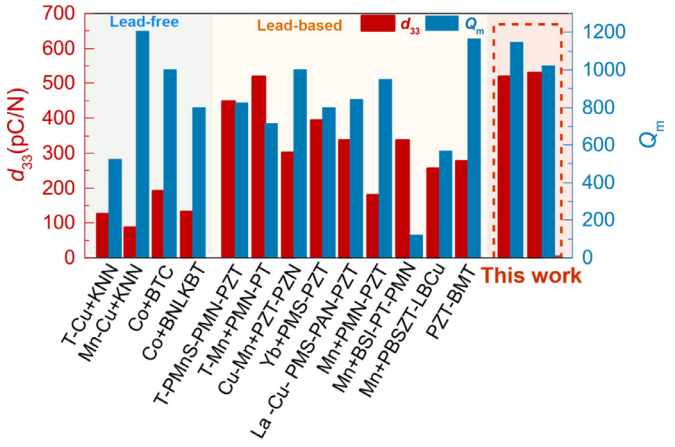

Fig. 1. Comparison of piezoelectric properties of high-power textured piezoelectric ceramics synthesized in this study with other lead-free and lead-based high-power piezoelectric ceramics in terms of d_{33} and Q_m (T denotes textured ceramic). [7,23,37,29–36]

been widely investigated due to their superior piezoelectric properties including high phase transition temperatures ($T_{r\text{-}t}$ and T_c) and high coercive field (E_c) in comparison with $Pb(Mg_{1/3}Nb_{2/3})O_3$-$PbTiO_3$ (PMN-PT) binary ferroelectrics. [24–26] Mn-doping is commonly used to induce the hard characteristics, [8,27,28] where Mn^{2+} or Mn^{3+} will substitute on B-site in perovskite structure creating oxygen vacancies. The oxygen vacancies diffuse to the domain wall region and pin the motion resulting in hard effect. In this study, 2 mol% MnO_2 doped PIN-PMN-PT ceramics were textured using TGG method. The effect of template content on <001> texturing degree, microstructure (grain size and density), and resulting dielectric and piezoelectric properties of textured Mn-doped PIN-PMN-PT ceramics is investigated. The domain structures of textured ceramic were characterized by piezoelectric force microscopy (PFM). Fig. 1 shows that textured Mn-doped PIN-PMN-PT ceramics can exhibit excellent soft and hard combinatory properties in comparison with random counterparts, and with other reported lead-free and lead-based high-power piezoelectric ceramics.

2. Experimental procedure

The matrix powder with the composition of 2 mol% MnO_2 doped 0.24 $Pb(In_{1/2}Nb_{1/2})O_3$-0.42 $Pb(Mg_{1/3}Nb_{2/3})O_3$-0.34 $PbTiO_3$ was synthesized using two-step columbite precursor method. [24,38] First, the raw materials of In_2O_3 (99.9%) and Nb_2O_5 (99.9%) were used to prepare $InNb_2O_4$ precursor at 1100 °C for 7 h. Next, the stoichiometric amounts of PbO (99.9%), $InNb_2O_4$, $MgNb_2O_6$ (99.9%), TiO_2 (99.8%), and MnO_2 (99.9%) were mixed in ethanol for 24 h. The dried mixtures were calcined at 850 °C for 4 h. Lastly, the calcined powders were ball milled again in ethanol for 72 h to decrease the particle sizes. $BaTiO_3$ (BT) templates were prepared by two-step topochemical microcrystal conversion (TMC) method. [39] First, the Bi_2O_3 (99.9%) and TiO_2 (99.8%) powders were mixed with salts (NaCl and KCl with a molar ratio of 1) and the mixtures were synthesized at 1050 °C for 2 h to obtain the lamellar structure $Bi_4Ti_3O_{12}$ (BiT) precursors. The BiT precursors and excess $BaCO_3$ were then mixed with alkali salts (NaCl and KCl with a molar ratio of 1) and synthesized at 970 °C for 2 h to obtain $BaTiO_3$ platelets. After that, the 2 mol% Mn-doped PIN-PMN-PT ceramics were textured by the templated grain growth (TGG) method using x vol.% BT templates (x = 1, 2, 3, 5). The samples are abbreviated as textured-xBT hereafter. The matrix powders, templates, organic binder, and toluene solvent were mixed to prepare the slurries for tape casting. The dried tapes were cut, stacked, and laminated to fabricate green samples. After binder burnout at 550 °C and cold-isostatic pressing at 200 MPa, the specimens were then embedded in calcined Mn-doped PIN-PMN-PT powders containing 1.5 wt% excess PbO within a closed crucible and sintered at 1220 °C for 6 h in air.

The crystal phases of the textured samples were determined using X-ray diffraction (XRD, PANalytical Empyrean). The degree of pseudocubic <001> texture F was determined by Lotgering factor method. [40,41]

$$F = \frac{P - P_0}{1 - P_0} \times 100\% \quad (1)$$

$$P = \frac{\Sigma I_{(00l)}}{\Sigma I_{(hkl)}} \quad (2)$$

$$P_0 = \frac{\Sigma I_{0(00l)}}{\Sigma I_{0(hkl)}} \quad (3)$$

Microstructures were evaluated using field-emission scanning electron microscopy (FESEM Apreo) in combination with energy dispersive spectroscopy (EDS) and electron backscatter diffraction (EBSD). For electrical measurements, the sample surfaces were polished and coated with silver paste. All the samples were poled at 40 kV/cm for 30 min at 140 °C. After aging for 48 h, the piezoelectric coefficient d_{33} was measured by using a d_{33} meter (YE2730A, APC Products). Temperature-dependent dielectric permittivity (ε_r), loss tangent (tan δ) and complex impedance were measured with a multifrequency LCR meter (Keysight E4980AL). Polarization vs. electric field (P-E) hysteresis loop was measured using a Precision PiezoMEMS analyzer (Radiant Technologies). The mechanical coupling coefficient (k) and mechanical quality factor (Q_m) were measured by resonance and anti-resonance technique using impedance analyzer (Keysight E4990A). Domain morphologies were characterized using the piezoelectric force microscopy (PFM) mode of a Bruker Icon II instrument.

3. Results and discussion

3.1. Fabrication of textured ceramics

Fig. 2 shows the morphology and XRD pattern of BT templates synthesized by TMC method. It can be found that the BT template has large anisotropy with 10 μm in length and 1 μm in thickness and exhibits tetragonal perovskite structure. These templates can be easily aligned under the applied shear force of doctor blade during tape casting process.

Fig. 3a shows the XRD patterns for both random and textured Mn-doped PIN-PMN-PT ceramics with different BT template contents. All samples exhibited perovskite structure without any noticeable secondary phase. With the introduction of BT template, the intensities of (00l) peaks increased rapidly while other peaks decreased significantly. Fig. 3b shows the texture degree as a function of BT template content. By increasing the BT content from 1 vol.% to 3 vol.%, the F_{00l} increases dramatically from 80% to 91% for Mn-doped PIN-PMN-PT. The texturing degree further increases to 95% by increasing the BT content to 5 vol.%. Fig. 3c shows the microstructures for both random and textured Mn-doped PIN-PMN-PT-3BT samples. Textured sample shows brick wall-like microstructures with well aligned BT templates (black areas) inside the oriented matrix grains, representing the development of texture, in comparison with the random ceramic with equiaxed grains. The <001>-textured Mn-doped PIN-PMN-PT was grown by a heteroepitaxial TGG process, which implies that the grown textured matrix grains have a different composition but small lattice mismatch (<0.6%) with template. The lattice match ensures

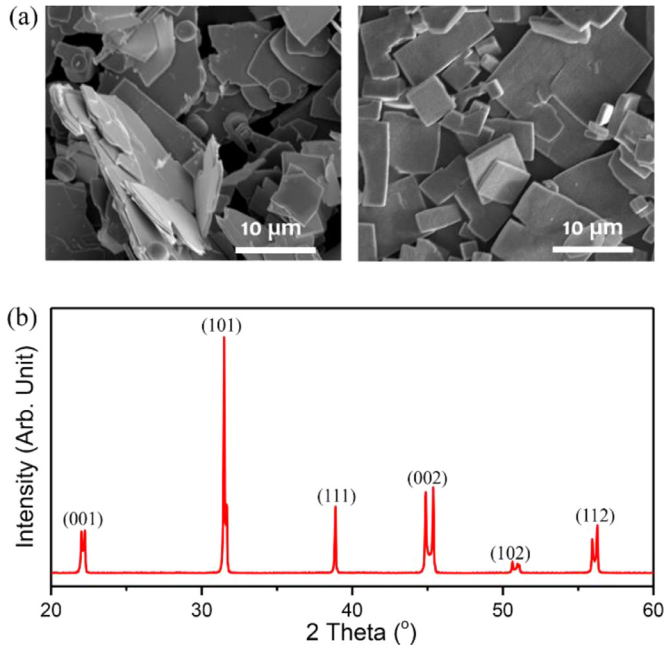

Fig. 2. (a) SEM images of $Bi_4Ti_3O_{12}$ (left) and $BaTiO_3$ (right); (b) XRD pattern of the $BaTiO_3$ templates.

the epitaxial nucleation of matrix Mn-doped PIN-PMN-PT grains on the lowest energy surface ({001}c plane) of BT template, resulting in the formation of <001>-textured grains. In order to provide understanding of the mechanism of templated grain growth, we collected a series of cross-sectional SEM images showing different stages of <001>-textured Mn-doped PIN-PMN-PT grains grown on the BT template during sintering process, as shown in Fig. S2. The large template size to matrix grain size ratio (>20) shown in Fig. S2a can generate a big difference in surface energy between the template and matrix grains, which is beneficial for providing the required driving force for textured grain growth. When the sample was held at high temperature, further heating will drive the rapid growth of textured grains. The textured grain growth is governed by Ostwald ripening process, where the large textured grains grow homoepitaxially via dissolution of finer matrix grains in PbO liquid layer and precipitation on the {001}c surface of textured grain. As a result, the <001>-textured grains grow at the expense of fine matrix grains. With further increase in the holding time at high temperature, the driving force for textured grain growth will decrease and the texture development becomes saturated. The reduced driving force is due to the matrix grain coarsening at high temperature, which decreases the ratio of template to matrix grain size. Finally, the large textured grains will impinge upon each other after critical growth distance and result in formation of <001>-textured Mn-doped PIN-PMN-PT ceramics.

EDS maps and line scan of textured ceramic are shown in Fig. 4. There is no noticeable interfacial reaction and diffusion at the interface between the matrix and BT template within the detection limit of EDS analysis, indicating that the BT template is highly stable inside the matrix. The EBSD inverse pole figure maps (Fig. 5) provide the evidence for high <001> orientation of grains in textured ceramic. In comparison, most of the grains are randomly oriented in random counterpart, which is consistent with results from the XRD (Fig. 3a).

3.2. Enhanced piezoelectric properties of textured ceramics

Fig. 6a and b show the dielectric constant, ε_r, and loss factor, tan δ, as a function of temperature for both random and textured Mn-doped PIN-PMN-PT samples. Two peaks corresponding to rhombohedral to tetragonal ($T_{r\text{-}t}$) and tetragonal to cubic (T_c) phase transitions can be observed in all samples. In addition, the first phase transition peak ($T_{r\text{-}t}$) becomes less obvious with increasing BT template, indicating the increased tetragonality degree of

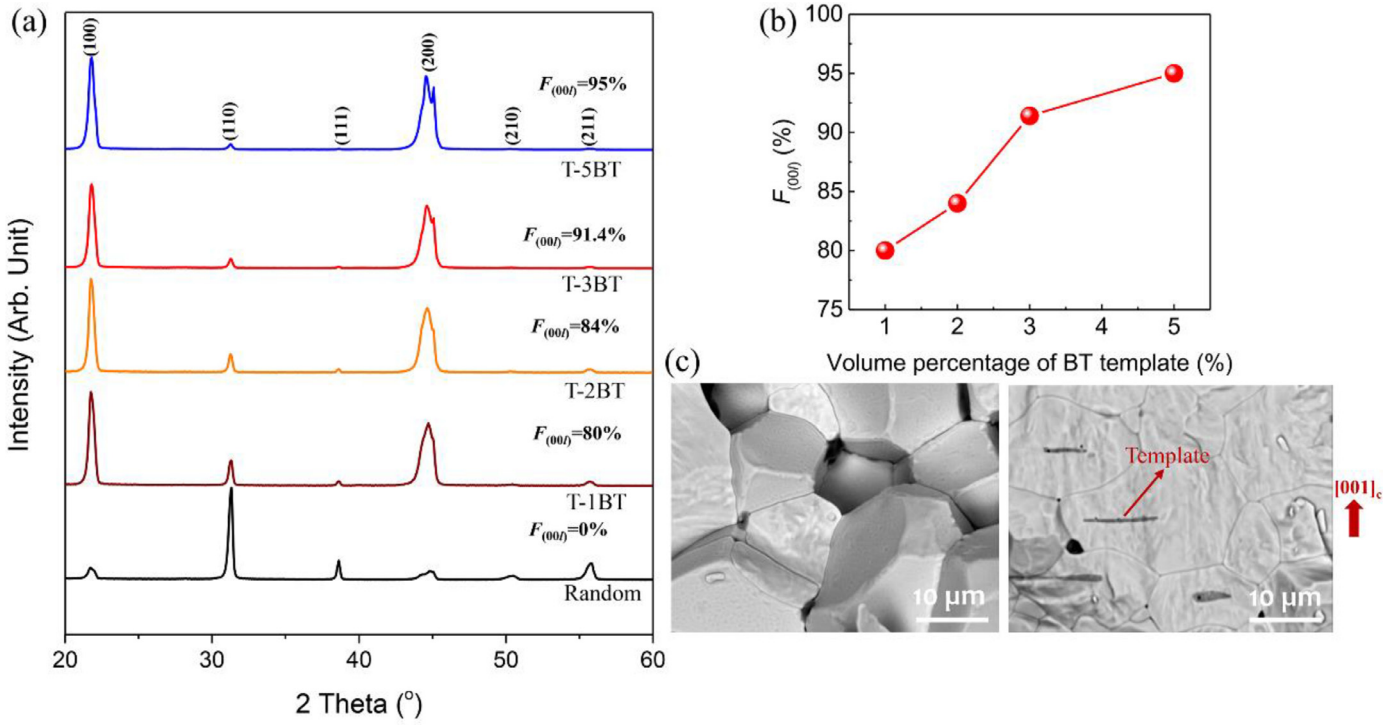

Fig. 3. (a) XRD patterns of Mn doped PIN-PMN-PT-*x*BT ceramics; (b) Texture degree $F_{(00l)}$ as a function of BT template content; (c) SEM micrographs of random (left) and Mn doped PIN-PMN-PT-3BT (right) ceramics.

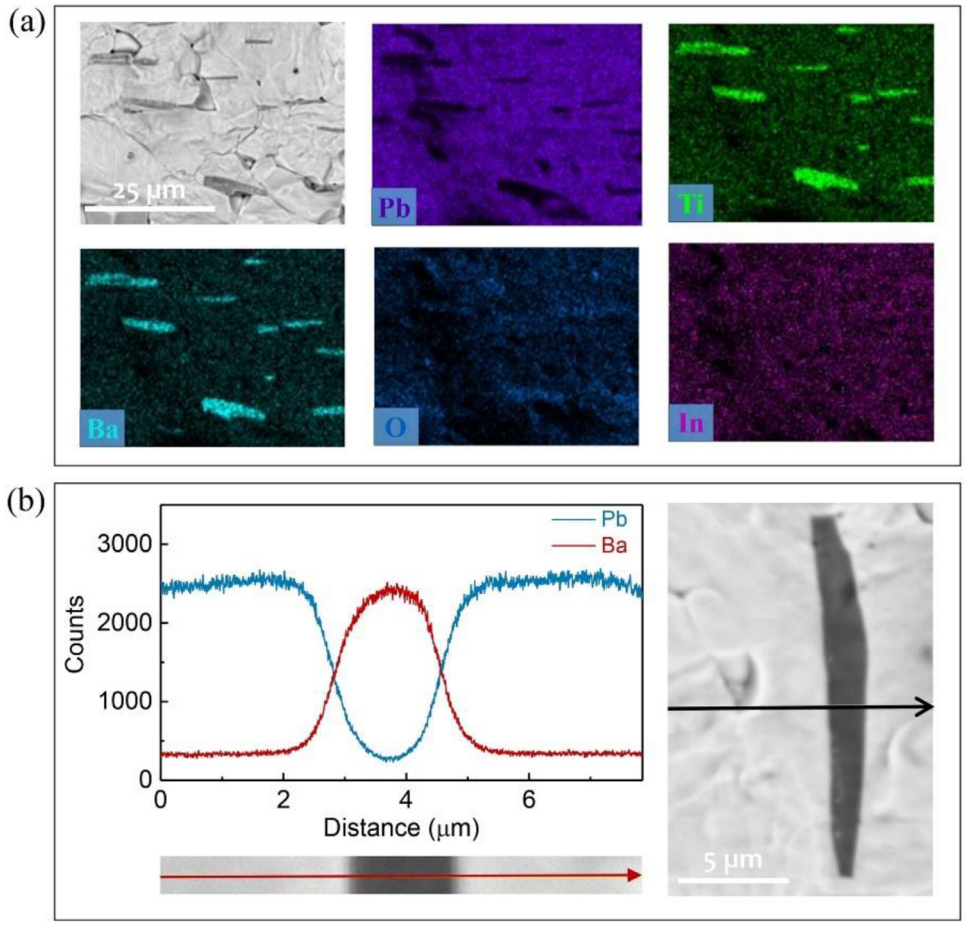

Fig. 4. (a) EDS element mapping of Mn doped PIN-PMN-PT- 3BT ceramic; (b) EDS line scan across the BT template inside the Mn-doped PIN-PMN-PT matrix.

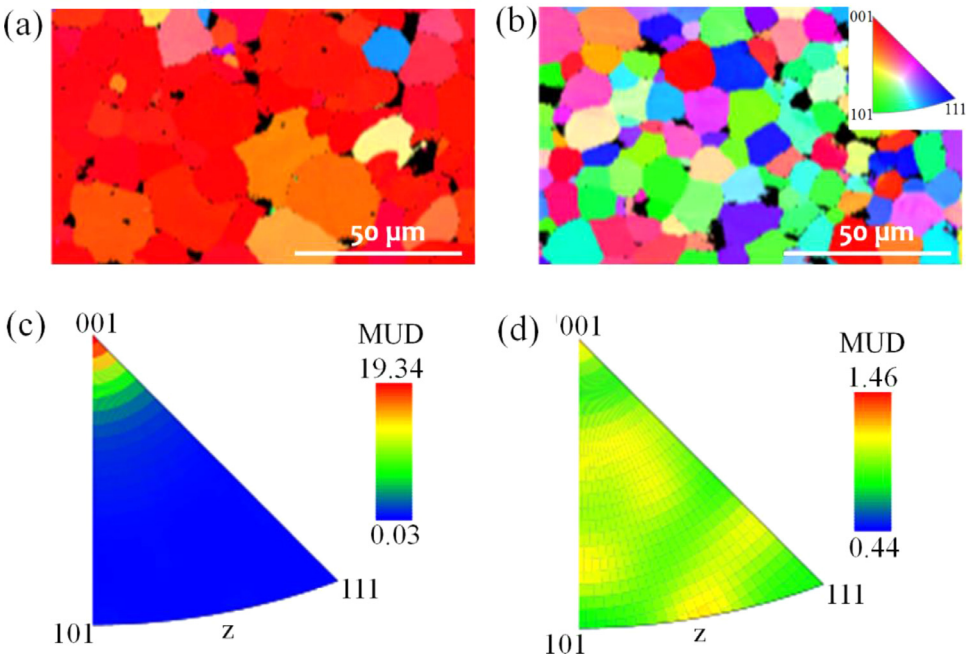

Fig. 5. EBSD images of (a) Mn-doped PIN-PMN-PT-3BT and (b) Mn-doped PIN-PMN-PT-0BT ceramics; (c) and (d) inversed pole figure with MUD (multiples uniform pole) data corresponding to (a) and (b), respectively.

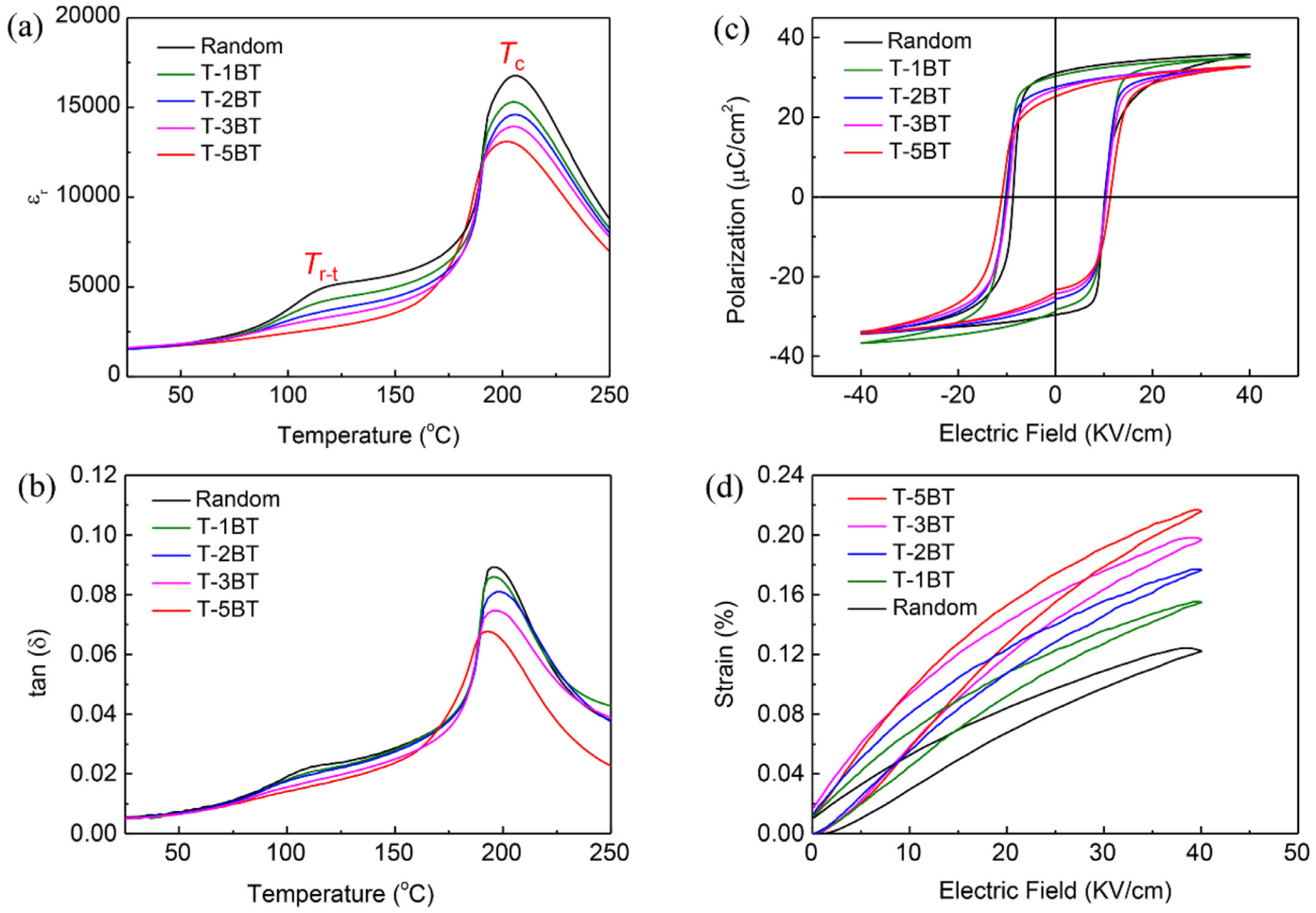

Fig. 6. Dielectric and piezoelectric properties: (a) Dielectric permittivity and (b) dielectric loss as a function of temperature for random and textured ceramics; (c) *P-E* hysteresis loops and (d) unipolar *S-E* curves for random and textured ceramics.

the sample. On the other hand, as the template content decreases, the Curie temperature T_c increases. The textured ceramics exhibit a high T_c above 200 °C, which is 30-70 °C higher than the binary PMN-PT ceramics [24,42], indicating the wider temperature use range for textured Mn-doped PIN-PMN-PT ceramics. Fig. 6c shows the *P-E* hysteresis loops for random and textured ceramics. All the samples exhibited well-saturated hysteresis loops under the electric field of 40 kV/cm. The textured ceramics possess lower remanent polarization (P_r) and higher coercive field (E_c) in comparison to their random counterparts. The lower P_r value can be explained by the composite effect of aligned BT template since the BT has been reported to exhibit a low P_r of 12 μC/cm^2. [43] The higher E_c can be attributed to the increased tetragonality of the sample with increasing BT content. Fig. 6d compares the unipolar strain-electric (*S-E*) curves for both textured and random ceramics. The textured ceramics exhibit almost ~2 times improvement in maximum strain S_m at the same electric field in comparison with random counterparts.

The temperature dependent XRD patterns for textured Mn-doped PIN-PMN-PT-3BT samples are shown in Fig. 7. The crystal structure is rhombohedral at room temperature. Above 100 °C, there is split in {002} peaks indicating that the rhombohedral phase gradually transforms to tetragonal phase (R-T phase transition). The non-polarized cubic phase can be observed at higher temperature, indicating the T-C phase transition when the measured temperature approaches T_c, which is consistent with the ε_r-*T* curve in Fig. 6a.

The detailed dielectric and piezoelectric properties for both random and textured piezoelectric ceramics are summarized in Table 1. The textured Mn-doped PIN-PMN-PT ceramics show improved piezoelectric properties with high T_c. Particularly, textured-2BT sample exhibited an excellent combination of soft and hard piezoelectric properties of d_{33} = 517 pC/N, Q_m = 1148, E_c = 10.0 kV/cm, along with high T_c around 205 °C in comparison with other reported high-power piezoelectric ceramics as shown in Fig. 1. These results indicate great potential of this composition for high-power piezoelectric applications. Fig. 8a shows the piezoelectric constant d_{33}, mechanical quality factor Q_m, and coercive field E_c as a function of BT template content. When $x \leq 3\%$, d_{33} increases rapidly with increasing *x*. The optimized value of 529 pC/N was obtained at $x = 3\%$, which is attributed to the improved texturing degree. [14,44]. However, with further increase of BT content to 5%, the d_{33} decreases to 475 pC/N. The reduced piezoelectric response is mainly attributed to the phase structure evolution. The magnification of XRD patterns in the range from 42° to 47° is shown in Fig. 8b, where the {002} peaks start to split with increasing BT content, indicating the increased tetragonality in textured ceramics. The direction of the spontaneous polarization in tetragonal and rhombohedral structure is along <001> and <111>, respectively (Fig. 8c). When an external electric field is applied along $[001]_c$ direction to the samples, the polarization will prefer to rotate in the same direction as that of the electric field. This results in the formation of domain configuration consisting of equivalent polar vectors along the electric field direction, known as domain engineer-

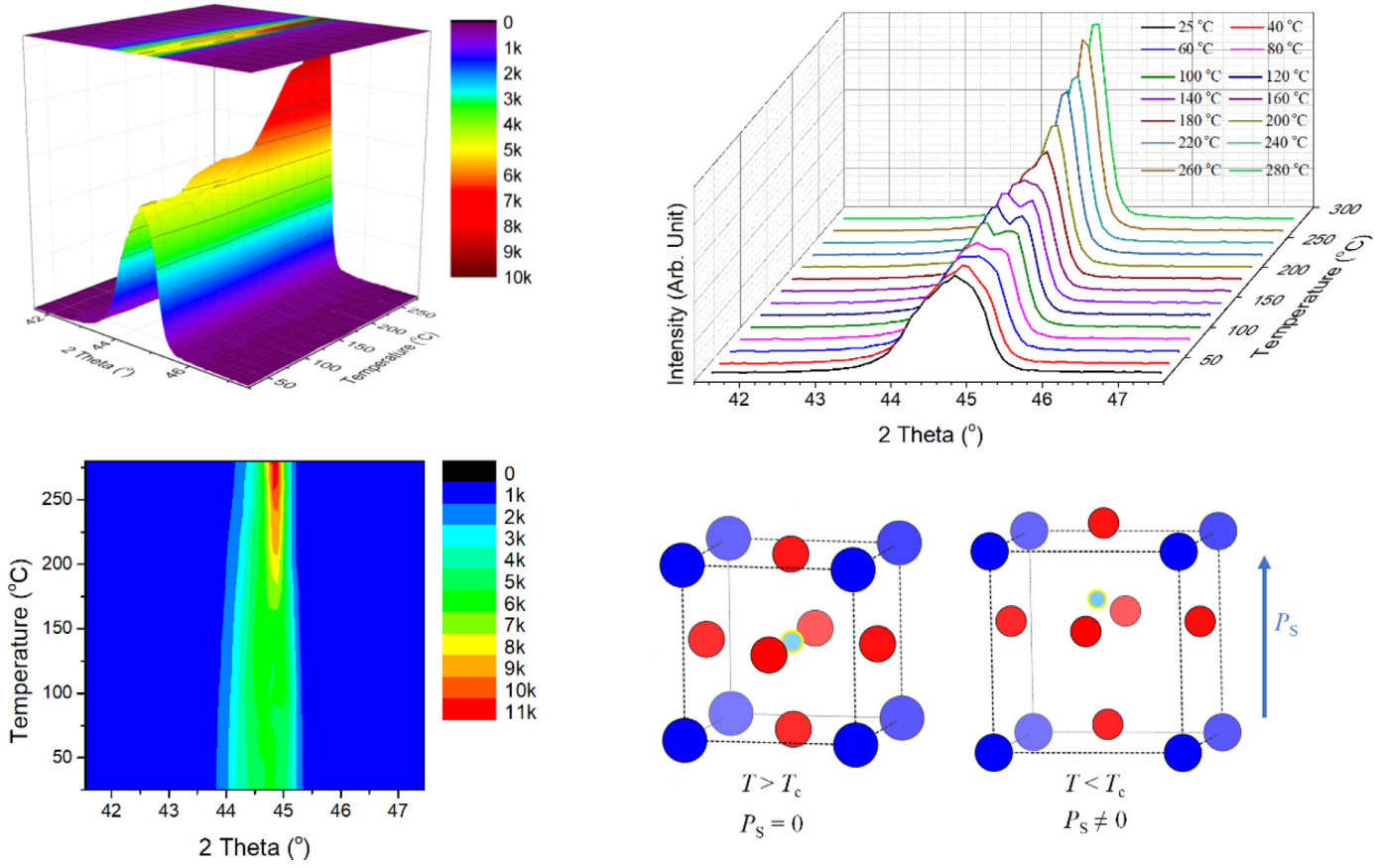

Fig. 7. Temperature dependence of XRD patterns for Mn-doped PIN-PMN-PT- 3BT ceramics.

Table 1
Dielectric and piezoelectric properties for both random and textured piezoelectric ceramics.

Specimen	F_{001} (%)	T_c (°C)	E_c (kV/cm)	$\varepsilon_{33}^T/\varepsilon_o$	*tan δ* (%)	d_{33} (pC/N)	d_{31} (pC/N)	k_{31}	Q_m
2 mol% Mn doped PIN-PMN-PT-0BT	0	213	9.4	1351	0.58	370	122	0.34	1693
2 mol% Mn doped PIN-PMN-PT-1BT	80	207	10.0	1422	0.47	457	155	0.40	1249
2 mol% Mn doped PIN-PMN-PT-2BT	84	205	10.0	1514	0.49	517	169	0.42	1148
2 mol% Mn doped PIN-PMN-PT-3BT	91	205	10.0	1520	0.49	529	175	0.42	1023
2 mol% Mn doped PIN-PMN-PT-5BT	95	199	11.4	1432	0.52	475	157	0.40	770

ing. [14,19,44] The engineered domain configuration explains the decreased piezoelectric response for textured ceramic with high BT content.

Both the number and orientation of the engineered domain configurations can influence the piezoelectric response. Prior studies have shown that the number (N) of equivalent engineered domain configurations and the angle (θ) between the external electric field and polarization direction in engineered domain configurations can directly influence the piezoelectric properties. [19,44,45] Usually, higher the number of equivalent domains and smaller is the angle, the higher will be the longitudinal piezoelectric response due to the easier polarization rotation under electric field. [19,44] In addition, among the two factors, the number of equivalent domains plays a more important role in influencing the piezoelectric response. [19] As shown in Fig. 9a, for <001>-oriented rhombohedral crystal, it has four equivalent engineered domains along with θ around 54.7°, while <001>-oriented tetragonal crystal only has one equivalent domain with θ around 0°. This implies that the tetragonal phase is less favorable to high longitudinal piezoelectric response in comparison with rhombohedral phase, which is consistent with our experimental results. The flattening of Gibbs free energy is believed to occur due to the multi-domain configuration, which can facilitate the polarization rotation. [3,46,47] <001>-oriented rhombohedral crystal exhibits flatter Gibbs free energy profile with lower energy barrier for polarization rotation in comparison with tetragonal counterpart (Fig. 9b), leading to an enhancement of piezoelectric response.

The reduced piezoelectric constant of textured sample with 5 vol.% BT templates is caused by the high tetragonality. The crystal structure of the textured sample gradually transforms into tetragonal structure with increasing x because the BT template has a tetragonal structure. For PMN-PT based ternary system, the coercive field value of the tetragonal structure is higher than that of the rhombohedral structure, [24,48,49] indicating that the domain rotation is difficult in tetragonal structure, which is consistent with our experimental results where the coercive field value E_c continuously increases with increasing x.

Domain structures play an important role in controlling the piezoelectric properties. [50–54] Thus, in order to uncover the mechanism for the enhanced piezoelectric properties of textured ceramic from the domain structure perspective, piezoresponse force microscopy (PFM) was performed for both random and textured samples. As shown in Fig. 10, all the samples exhibit an island-type domain structure. Specifically, the textured-3BT sam-

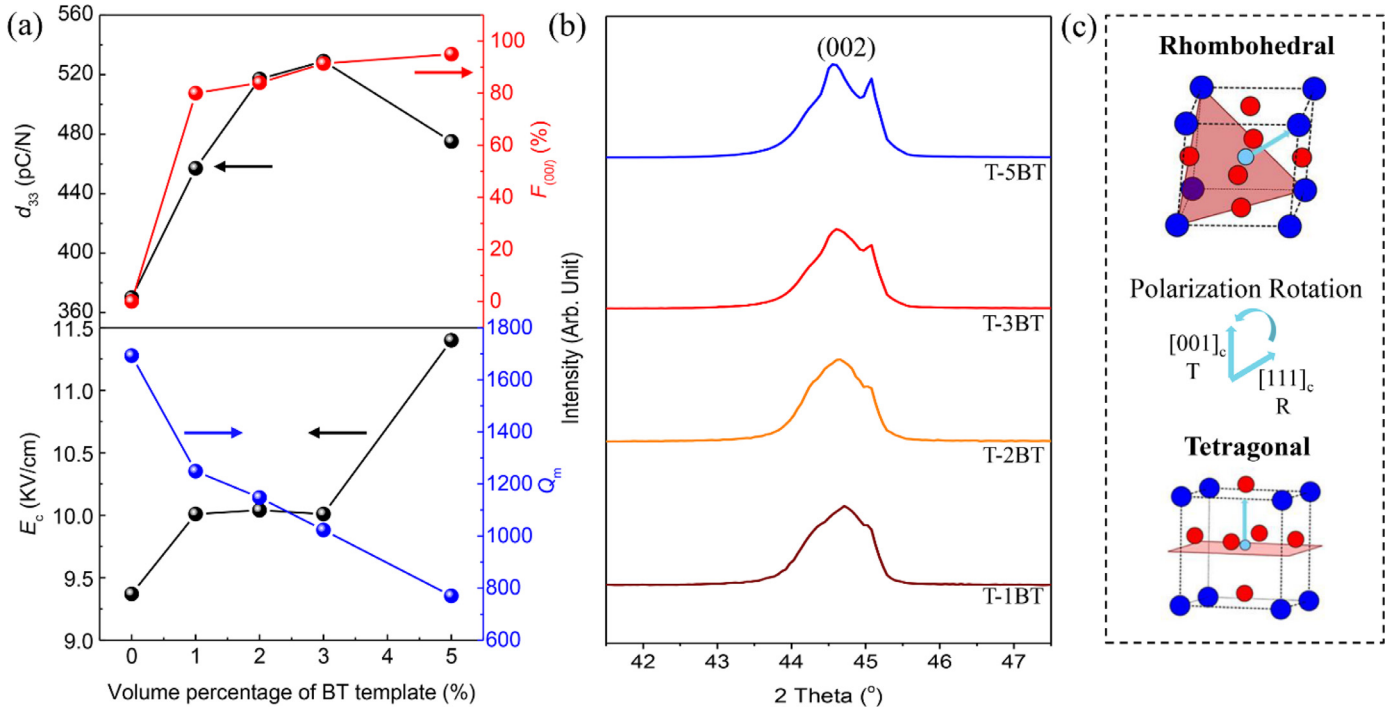

Fig. 8. (a) The piezoelectric constant d_{33}, mechanical quality factor Q_m, and coercive field E_c as a function of BT template content; (b) the magnification of XRD patterns of Mn-doped PIN-PMN-PT-*x*BT ceramic in the range from 42° to 47°; (c) polarization rotation between rhombohedral and tetragonal crystal structure.

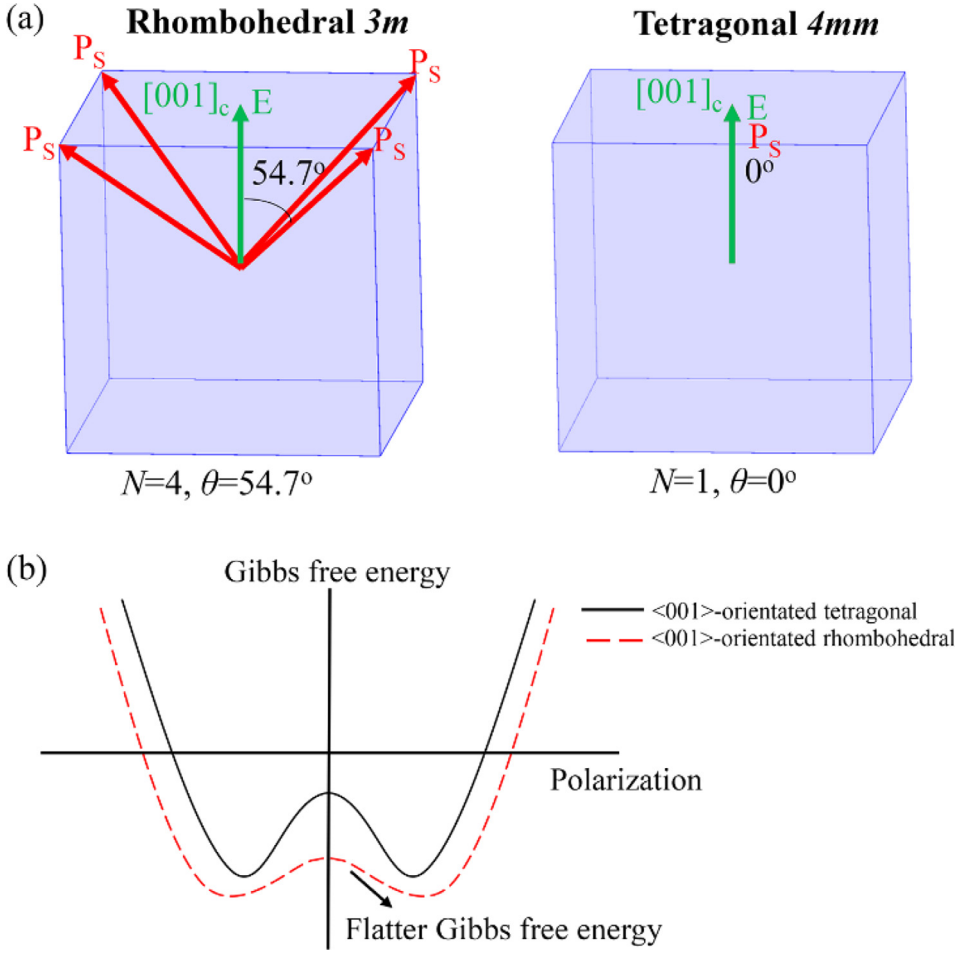

Fig. 9. (a) Engineered domain configurations and (b) free energy for [001]c-orientated rhombohedral and tetragonal crystals.

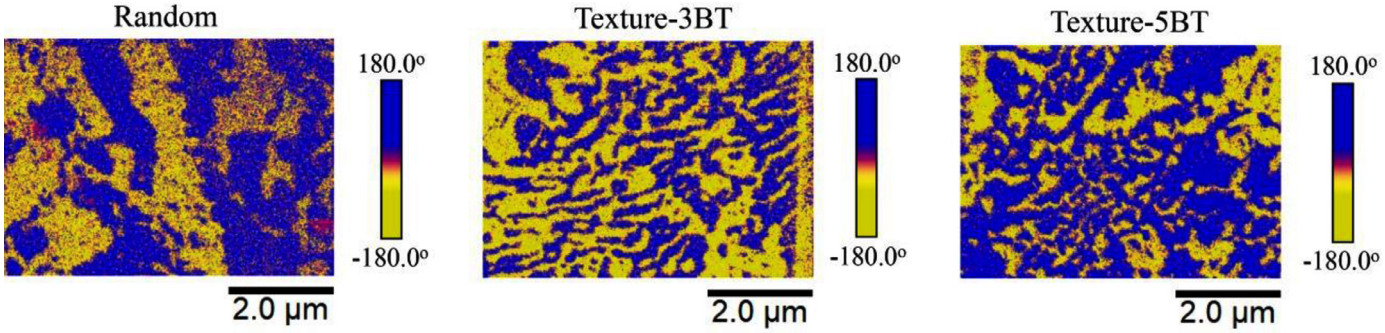

Fig. 10. Vertical piezoresponse force microscopy (VPFM) images of both random and textured piezoelectric ceramics.

ple has the smallest and homogeneous domain in comparison with both textured-5BT and random samples, while the random sample exhibits the largest domain size. According to the prior studies, [54–56] the domain size D is proportional to the square root of domain wall energy ($D \propto \sqrt{\gamma}$). Thus, the finer and uniform domains in textured samples can promote the domain wall motion and domain switching under external electric field due to their decreased domain wall energy and increased flexibility in comparison with large size domains in random counterpart, leading to enhanced piezoelectric response. Thus, the improved piezoelectric performance of textured-3BT sample can also be attributed to the formation of finer and uniform domains. Domain formation will minimize the elastic energy in piezoelectric ceramics. [57] In textured ceramics, both the grain boundaries, heterogeneous templates and stress from the epitaxial textured grain-template interfaces can influence the total elastic energy of the piezoelectric systems. [42] These perturbations in elastic energy will lead to the formation of fine size domains in textured ceramics in order to reduce the overall energy of the system. It is interesting to find that the textured-5BT sample also exhibits the stripe domain structure besides the island-type domains, which is shown in Fig. S5, indicating the high tetragonality of the sample since the tetragonal structure usually exhibits stripe-type domains. The existence of the stripe domain structure further confirms the high tetragonality of the textured-5BT sample, which agrees well with the XRD pattern shown in Fig. 8b.

3.3. Origin of improved mechanical quality factor

The mechanical quality factor Q_m decreases as the BT content increases as shown in Fig. 8a. The random sample exhibited a high Q_m value of 1693. It is known that the high Q_m value is closely related to the internal bias field E_i. Fig. 11a shows an acceptor-doped perovskite crystal lattice with a polarization P_D induced by defect dipole. For example, in Mn-doped piezoelectric ceramics, Mn^{2+} or Mn^{3+} ion will substitute on the B-sites of the perovskite structure, such as Nb^{5+} and Ti^{4+}, depending upon the crystal symmetry. [58–60] In a polar ferroelectric phase, the center B-site ion displaces towards the upper oxygen atom, generating a spontaneous polarization P_S with a direction parallel to the displacement, as shown in Fig. 11a. The acceptor substitution on B-sites will generate negatively charged defects paired with oxygen vacancies due to the charge neutrality, resulting in the formation of defect dipoles such as $Mn_{Ti}'' - V_O^{\cdot\cdot}$. Considering the polar phase symmetry, the surrounding oxygen neighbors are nonequivalent sites with respect to the center defect ion induced by acceptor doping, leading to the unequal probability of producing oxygen vacancy in oxygen neighbors. Compared to other oxygen neighbors, the upper oxygen site has a higher probability of generating oxygen vacancy (P_V) because it is closer to the center of negatively charged defect ion (Fig. 11a). As a result, electric dipole moment has the same direction as the spontaneous polarization P_S and the defect dipole induced P_D will be along P_S direction. Prior electron paramagnetic resonance (EPR) results further confirm that the defect dipoles prefer to align in the same direction as spontaneous polarization P_S. [61–63] Since oxygen diffusion process is thermally activated and the mobility of oxygen vacancy is slow at room temperature, [64] the reorientation of defect dipoles will be harder under the external electric field. Thus, the P_D will be stable while the P_S will be changed by the electric field. The energy state of upward $+P_S$ and downward $-P_S$ polarization is nonequivalent owing to the existence of irreversible defect dipoles, leading to an energy gap $\Delta E>0$, which is shown in Fig. 11b.

Following the relationship between the polarization and electric field in dielectric materials, [65] an electric bias E_D can be induced by the defect polarization P_D, which is shown in the equation: [66]

$$E_D = \frac{P_D}{\varepsilon_0 \chi} \tag{4}$$

where ε_0 is the vacuum permittivity, χ is the dielectric susceptibility; the induced E_D has the same direction as P_D and its value is directly proportional to the magnitude of P_D. To switch the polarization of acceptor-doped piezoelectric ceramics, the applied electric field E_{ex} should exceed the sum of E_c and E_D, where the E_D can be parallel or antiparallel to E_c, resulting in an asymmetric P-E hysteresis loop (Fig. 11c). In addition, the internal bias field E_i can be generated due to the switching of defect dipoles in acceptor-doped piezoelectric ceramics. [67] The relationship between the E_D and E_i can be expressed as: [66]

$$E_i = E_D \cdot \cos\theta \tag{5}$$

where θ is the angle between the electric field and the spontaneous polarization. Note, E_i can be equal to E_D only when the applied electric field follows the direction of spontaneous polarization. In our case, the piezoelectric ceramic has a multi-domain configuration and the applied electric field is not parallel to the polarization direction. Thus, the defect dipoles can restrict both polarization rotation and extension, which is illustrated in Fig. 11d. The induced E_i can be decomposed into two components $E_\parallel$ and $E_\perp$, where $E_\parallel$ and $E_\perp$ are parallel and perpendicular to the direction of P_S, respectively (Fig. 11e), and θ is the angle between the electric field and the polarization. The $E_\parallel$ and $E_\perp$ can be obtained as:

$$E_\parallel = E_i \cdot \cos\theta \tag{6}$$

$$E_\perp = E_i \cdot \sin\theta \tag{7}$$

when $\theta \neq 0$, and both $E_\parallel$ and $E_\perp$ are positive. The $E_\parallel$ can restrict the polarization extension. The induced force moment from $E_\perp$ will

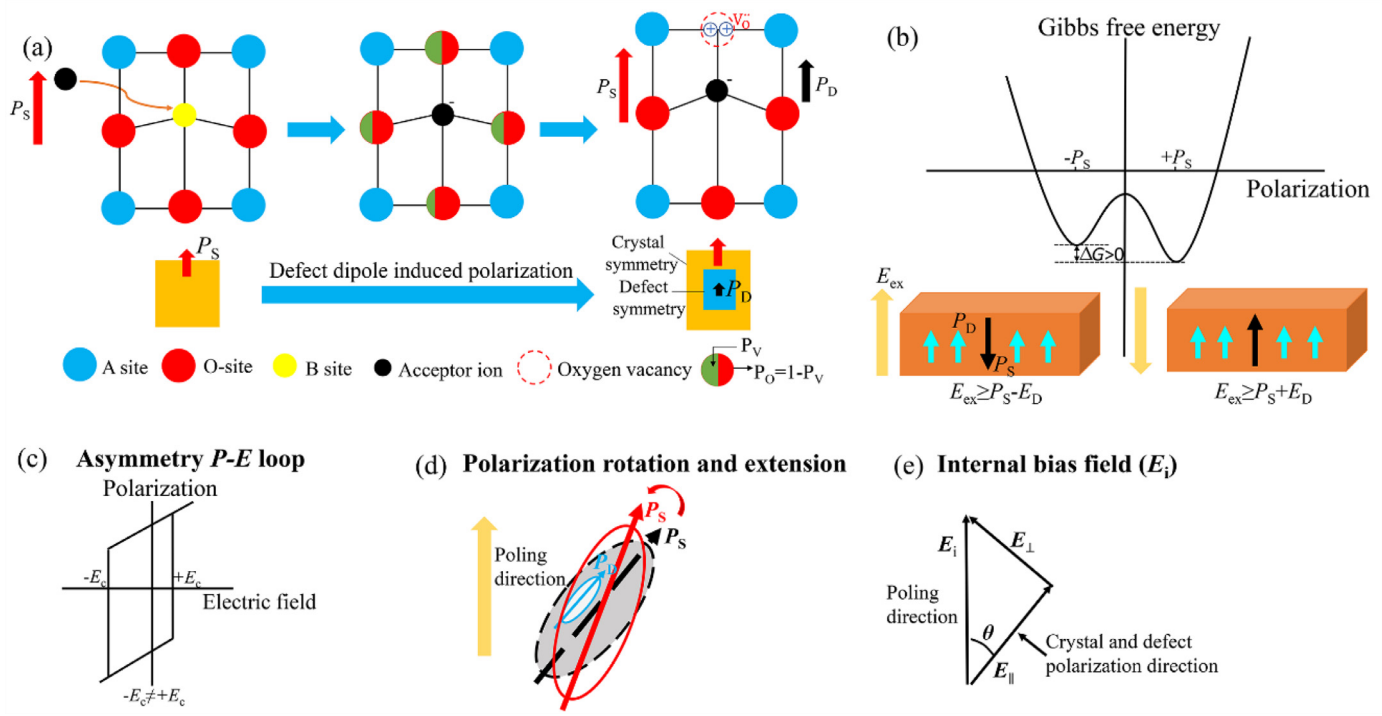

Fig. 11. (a) Development of defect polarization P_D in acceptor-doped ABO_3 perovskite lattice; (b) free energy with non-zero energy gap and (c) asymmetric *P-E* loop induced by defect dipoles; (d) polarization rotation and extension in acceptor-doped piezoelectrics; (e) internal bias field E_i along with two components $E_\parallel$ and $E_\perp$ parallel and perpendicular to crystal/defect polarization direction, respectively.

prevent the polarization rotation, resulting in large reduction and enhancement in piezoelectric response and Q_m, respectively. In addition, according to Eqn (5), the magnitudes of $E_\parallel$ and $E_\perp$ component are proportional to value of E_D. Thus, a large E_D will induce a large variation in piezoelectric properties. The magnitude of E_D is affected by both valence state and content of acceptor ion. As a result, the 2 mol% Mn-doped PIN-PMN-PT ceramic has a larger E_i value around 1.59 kV/cm, in comparison with 1 mol% Mn-doped counterpart (E_i ~ 0.32 kV/cm), since the high content acceptor ion can induce larger P_D and E_D, as shown in Fig. S4. The E_i value can be calculated by $E_i = (E_{c+} + E_{c-})/2$, where E_{c+} and E_{c-} are the intersections of the polarization loop with the positive and negative electric field axis, respectively. A larger E_i will generate enhanced restriction on polarization extension and rotation, resulting in a lower d_{33} of 370 pC/N and much higher Q_m of 1693 for 2mol% Mn-doped ceramic in comparison with 1 mol% Mn-doped counterpart exhibiting values of d_{33} = 450 pC/N, Q_m = 745. Thus, the high mechanical quality factor Q_m value of random sample is caused by the large internal bias field E_i. The reason for the reduced Q_m of textured ceramics is discussed below.

Fig. 12 shows the complex impedance plots for both random and textured samples over the temperature ranges of 400-600 °C. All the plots show the similar behavior. The bulk resistance corresponds to the low frequency intercept of the impedance plot on the Z′ axis and the ionic conductivity was calculated in accordance with the literature. [68,69] The activation energy E_a can be calculated using Arrhenius equation:

$$\sigma = \sigma_0 \exp(-E_a/KT) \quad (8)$$

where σ is conductivity, σ_0 is pre exponential factor, E_a is the activation energy of the conduction, K is the Boltzmann constant, and T is the absolute temperature.

From the lnσ vs. 1000/T curves, the E_a for the 1 mol% Mn-doped random, 2 mol% Mn-doped random, textured-2BT, and textured-5BT samples is calculated to be 1.51 eV, 1.18 eV, 1.24 eV, and 1.23 eV, respectively. Random sample with 2 mol% Mn-doping exhibits a much lower activation energy value in comparison with 1 mol% Mn-doped random sample since more Mn ions will substitute on the B-site of the perovskite structure, generating high concentration of oxygen vacancies in 2 mol% Mn-doped sample. However, the differences in activation energy for both random and textured samples are small, indicating that the mobility or concentration of oxygen vacancies may not be the key factor to induce the different Q_m value in random and textured samples. The reduced Q_m of <001>-textured ceramics in comparison with random counterpart could be caused by the crystallographic dependence of Q_m in PIN-PMN-PT ceramics. Previously, it has been reported that the Q_m reached the high value of 1100 for <111> oriented rhombohedral PIN-PMN-PT single crystal and exhibited the smaller value of 120 for <001> oriented counterpart. [70] This crystallographic dependence of Q_m was attributed to the different domain engineered configurations for different orientations. For electric poled <111>-oriented crystal, the domain engineered structure is monodomain, labeled as 1R, thus low elastic loss and high Q_m are expected. For electrically poled <001>-oriented crystal, it has four equivalent engineered domains along with θ around 54.7° as shown in Fig. 9a, designated as 4R, leading to enhanced domain wall motion and high elastic loss. Thus, the higher Q_m for <111>-oriented crystal with domain engineered configuration 1R in comparison with <001>-oriented counterpart is attributed to the reduced domain wall motion. Considering the averaging of Q_m in three-dimensional space, the random sample should have a Q_m in between that of <001> and <111>-textured ceramics. Thus, it is reasonable to see that the <001>-textured ceramics have lower Q_m in comparison with random counterpart by considering the crystallographic dependence of Q_m.

Further, based on PFM phase images shown in Fig. 10, the existence of small and uniform domains makes the domain switching relatively easier to happen in textured sample. Thus, the crystallographic dependence of Q_m and enhanced domain mobility may

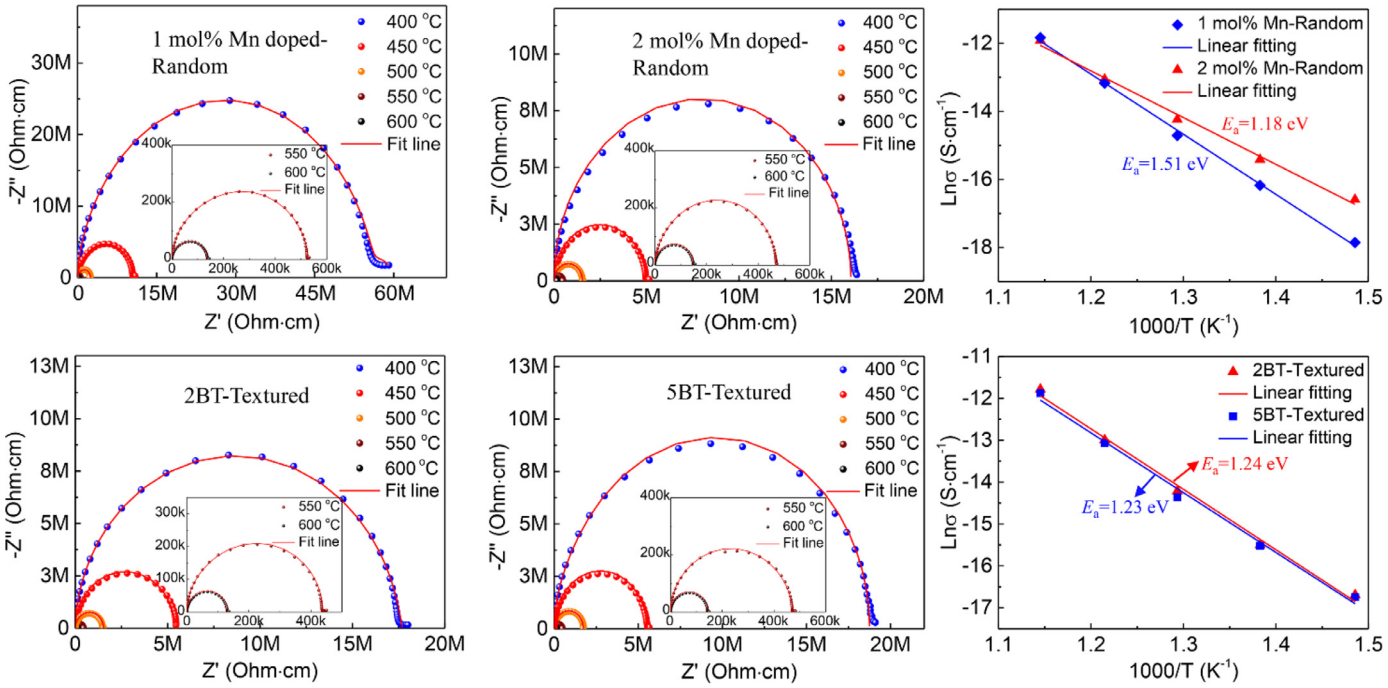

Fig. 12. Temperature dependent complex impedance spectra and corresponding Arrhenius plots of ionic conductivities for both random and textured piezoelectric ceramics.

be the main reasons why the mechanical quality factor Q_m decreased as the BT content increased. In addition, the multi-domain configuration will gradually transfer to single domain configuration with increasing BT content since the BT template can increase the tetragonality of textured ceramic. For single domain configuration, the angle θ between the electric field and the polarization is zero, based on Eqn. 6 and 7, when $\theta = 0$, $E_\perp = 0$. Thus, only the parallel component of internal bias field $E_\parallel$ can restrict the extension of polarization, leading to the decreased Q_m.

4. Conclusion

High power piezoelectric ceramics have been successfully fabricated using integrated texturing and acceptor doping (Mn-doping). The mechanism for the enhanced piezoelectric response of textured ceramic is attributed to the high <001>-crystal orientation and fine domain structure. The effect of template content on piezoelectric properties of textured ceramics was investigated and the results show that the BT template content in textured ceramic should not exceed 3 vol.% in order to achieve an optimized combined soft and hard piezoelectric properties. Template content higher than 3 vol.% can increase the tetragonality degree of textured ceramic, resulting in decreased piezoelectric coefficient. Also, the high template content can significantly reduce the mechanical quality factor value of textured ceramic since the high content of BT template can transform the multi-domain configuration to single domain configuration due to the phase transition from rhombohedral to tetragonal structure, leading to reduced restriction on polarization motion and decreased mechanical quality factor. The textured Mn-doped PIN-PMN-PT with 2 vol.% BT template exhibited excellent piezoelectric properties of $d_{33} = 517$ pC/N, $Q_m = 1147$, $E_c = 10.0$ kV/cm, tan $\delta = 0.49\%$, which is higher than most of the reported lead-free and lead-based high-power piezoelectric ceramics. We believe that the outstanding piezoelectric properties of textured Mn-doped PIN-PMN-PT with low production cost make it promising for next-generation high power devices applications.

Declaration of Competing Interest

The authors declare that they have no known competing financial interests or personal relationships that could have appeared to influence the work reported in this paper.

The authors declare the following financial interests/personal relationships which may be considered as potential competing interests.

Acknowledgements

The authors acknowledge the financial support from DARPA through award number HR00111920001. Y.Y. and S.P. acknowledge the partial support through National Science Foundation instrumentation grant with award number 1828609. We thank Yuchen Hou for his assistance with PFM measurements. The authors would like to thank Dr. Harold C. Robinson for helpful discussions throughout this study.

Supplementary materials

Supplementary material associated with this article can be found, in the online version, at doi:10.1016/j.actamat.2020.116610.

References

[1] M.B. Starr, X. Wang, Coupling of piezoelectric effect with electrochemical processes, Nano Energy 14 (2014) 296–311, doi:10.1016/j.nanoen.2015.01.035.
[2] M. Slabki, J. Wu, M. Weber, P. Breckner, D. Isaia, K. Nakamura, J. Koruza, Anisotropy of the high-power piezoelectric properties of Pb(Zr,Ti)O 3, J. Am. Ceram. Soc. 102 (2019) 6008–6017, doi:10.1111/jace.16464.
[3] T. Zheng, J. Wu, D. Xiao, J. Zhu, Recent development in lead-free perovskite piezoelectric bulk materials, Prog. Mater. Sci. 98 (2018) 552–624, doi:10.1016/j.pmatsci.2018.06.002.
[4] A.M. Manjón-Sanz, M.R. Dolgos, Applications of Piezoelectrics: Old and New, Chem. Mater 30 (2018) 8718–8726, doi:10.1021/acs.chemmater.8b03296.
[5] H.Y. Park, C.H. Nam, I.T. Seo, J.H. Choi, S. Nahm, H.G. Lee, K.J. Kim, S.M. Jeong, Effect of MnO2 on the piezoelectric properties of the 0.75Pb(Zr0.47Ti0.53)O3-0.25Pb(Zn 1/3Nb2/3)O3 ceramics, J. Am. Ceram. Soc. 93 (2010) 2537–2540, doi:10.1111/j.1551-2916.2010.03888.x.
[6] Y. Yan, K.H. Cho, S. Priya, Piezoelectric properties and temperature stability of Mn-doped Pb(Mg 1/3Nb 2/3)-PbZrO 3-PbTiO 3 textured ceramics, Appl. Phys. Lett. (2012) 100, doi:10.1063/1.3698157.

[7] H.J. Lee, S.O. Ural, L. Chen, K. Uchino, S. Zhang, High power characteristics of lead-free piezoelectric ceramics, J. Am. Ceram. Soc. 95 (2012) 3383–3386, doi:10.1111/j.1551-2916.2012.05462.x.

[8] S. Zhang, S.M. Lee, D.H. Kim, H.Y. Lee, T.R. Shrout, Characterization of Mn-modified Pb (Mg13 Nb23)O 3 -PbZrO3 -PbTiO3 single crystals for high power broad bandwidth transducers, Appl. Phys. Lett. 93 (2008) 1–4, doi:10.1063/1.2992081.

[9] D. Lin, K.W. Kwok, H.L.W. Chan, Piezoelectric properties and hardening behavior of K5.4 Cu 1.3 Ta10 O29 -doped K0.5 Na 0.5 Nb O3 ceramics, J. Appl. Phys. 103 (2008) 0–5, doi:10.1063/1.2896588.

[10] L. Zheng, L. Yang, Y. Li, X. Lu, D. Huo, W. Lü, R. Zhang, B. Yang, W. Cao, Origin of Improvement in Mechanical Quality Factor in Acceptor-Doped Relaxor-Based Ferroelectric Single Crystals, Phys. Rev. Appl. 9 (2018) 64028, doi:10.1103/PhysRevApplied.9.064028.

[11] S. Zhang, R. Xia, L. Lebrun, D. Anderson, T.R. Shrout, Piezoelectric materials for high power, high temperature applications, Mater. Lett. 59 (2005) 3471–3475, doi:10.1016/j.matlet.2005.06.016.

[12] F.H. Schader, G.A. Rossetti, J. Luo, K.G. Webber, Piezoelectric and ferroelectric properties of <001>C Pb(In1/2Nb1/2)O3-Pb(Mg1/3Nb2/3)O3-PbTiO3 single crystals under combined thermal and mechanical loading, Acta Mater 126 (2017) 174–181, doi:10.1016/j.actamat.2016.12.051.

[13] S.E.E. Park, W. Hackenberger, High performance single crystal piezoelectrics: Applications and issues, Curr. Opin. Solid State Mater. Sci. 6 (2002) 11–18, doi:10.1016/S1359-0286(02)00023-2.

[14] A.D. Moriana, S. Zhang, Lead-free textured piezoceramics using tape casting: A review, J. Mater. 4 (2018) 277–303, doi:10.1016/j.jmat.2018.09.006.

[15] S.F. Poterala, Closing The Performance Gap Between< 001>c Textured Pmn-pt ceramics And Single Crystals (2012).

[16] E.M. Sabolsky, A.R. James, S. Kwon, S. Trolier-McKinstry, G.L. Messing, Piezoelectric properties of '001' textured Pb(Mg1/3Nb2/3)O3-PbTiO3ceramics, Appl. Phys. Lett. 78 (2001) 2551–2553, doi:10.1063/1.1367291.

[17] Y. Chang, B. Watson, M. Fanton, R.J. Meyer, G.L. Messing, Enhanced texture evolution and piezoelectric properties in CuO-doped Pb(In1/2Nb1/2)O3-Pb(Mg1/3Nb2/3)O3-PbTiO3 grain-oriented ceramics, Appl. Phys. Lett. (2017) 111, doi:10.1063/1.5006288.

[18] Y. Chang, Y. Sun, J. Wu, X. Wang, S. Zhang, B. Yang, G.L. Messing, W. Cao, Formation mechanism of highly [0 0 1] c textured Pb(In 1/2 Nb 1/2)O 3 -Pb(Mg 1/3 Nb 2/3)O 3 -PbTiO 3 relaxor ferroelectric ceramics with giant piezoelectricity, J. Eur. Ceram. Soc. 36 (2016) 1973–1981, doi:10.1016/j.jeurceramsoc.2016.02.030.

[19] P. Li, J. Zhai, B. Shen, S. Zhang, X. Li, F. Zhu, X. Zhang, Ultrahigh Piezoelectric Properties in Textured (K,Na)NbO3-Based Lead-Free Ceramics, Adv. Mater. 30 (2018) 1–9, doi:10.1002/adma.201705171.

[20] G.L. Messing, S. Trolier-McKinstry, E.M. Sabolsky, C. Duran, S. Kwon, B. Brahmaroutu, P. Park, H. Yilmaz, P.W. Rehrig, K.B. Eitel, E. Suvaci, M. Seabaugh, K.S. Oh, Templated grain growth of textured piezoelectric ceramics (2004), doi:10.1080/10408430490490905.

[21] Y. Yan, Y.U. Wang, S. Priya, Electromechanical behavior of [001]-textured Pb(Mg1/3Nb2/3)O3-PbTiO3 ceramics, Appl. Phys. Lett. (2013) 192905.

[22] Y. Yan, J.E. Zhou, D. Maurya, Y.U. Wang, S. Priya, Giant piezoelectric voltage coefficient in grain-oriented modified PbTiO 3 material, Nat. Commun. 7 (2016) 1–10, doi:10.1038/ncomms13089.

[23] H. Liu, Y. Yan, H. Leng, A. Heitmann, J.B. Blottman, S. Priya, High performance high power textured piezoceramics, Appl. Phys. Lett. 116 (2020), doi:10.1063/5.0009501.

[24] D. Wang, M. Cao, S. Zhang, Phase diagram and properties of Pb(In1/2Nb1/2)O3-Pb(Mg1/3Nb2/3)O3-PbTiO3 polycrystalline ceramics, J. Eur. Ceram. Soc. 32 (2012) 433–439, doi:10.1016/j.jeurceramsoc.2011.08.025.

[25] D. Wei, H. Wang, Low-temperature sintering and enhanced piezoelectric properties of random and textured PIN–PMN–PT ceramics with Li2CO3, J. Am. Ceram. Soc. 100 (2017) 1073–1079, doi:10.1111/jace.14657.

[26] B.H. Watson, M.J. Brova, Y. Chang, S.T. Misture, M.A. Fanton, R.J. Meyer, G.L. Messing, Low temperature reactive sintering of CuO-doped PIN-PMN-PT ceramics, J. Eur. Ceram. Soc. 39 (2019) 4719–4726, doi:10.1016/j.jeurceramsoc.2019.06.030.

[27] Y. Yan, K.H. Cho, S. Priya, Identification and effect of secondary phase in MnO2-doped 0.8Pb(Zr0.52Ti0.48)O3-0.2Pb(Zn 1/3Nb2/3)O3 piezoelectric ceramics, J. Am. Ceram. Soc. 94 (2011) 3953–3959, doi:10.1111/j.1551-2916.2011.04629.x.

[28] X. Qi, E. Sun, J. Wang, R. Zhang, Bin Yang, W. Cao, Electromechanical properties of Mn-doped Pb(In1/2Nb1/2)O3-Pb(Mg1/3Nb2/3)O3-PbTiO3 piezoelectric ceramics, Ceram. Int. 42 (2016) 15332–15337, doi:10.1016/j.ceramint.2016.06.175.

[29] B. Zhang, H. Qi, R. Zuo, A new low-temperature firable 0.95Pb(ZrxTi1-x)O3-0.05Bi(Mn1/2Ti1/2)O3 ceramic for high-power applications, Ceram. Int. 44 (2018) 5453–5458, doi:10.1016/j.ceramint.2017.12.178.

[30] S.F. Poterala, S. Trolier-Mckinstry, R.J. Meyer, G.L. Messing, Processing, texture quality, and piezoelectric properties of 001 C textured (1-x)Pb(Mg1/3Nb2/3)TiO3 - XPbTiO3 ceramics, J. Appl. Phys. (2011) 110, doi:10.1063/1.3603045.

[31] C.H. Nam, H.Y. Park, I.T. Seo, J.H. Choi, S. Nahm, H.G. Lee, Effect of CuO on the sintering temperature and piezoelectric properties of MnO2-doped 0.75Pb(Zr0.47Ti0.53)O 3-0.25Pb(Zn1/3Nb2/3)O3 ceramics, J. Alloys Compd. 509 (2011) 3686–3689, doi:10.1016/j.jallcom.2010.12.163.

[32] Z. Zhu, G. Li, B. Li, Q. Yin, K. Jiang, The influence of Yb and Nd substituents on high-power piezoelectric properties of PMS-PZT ceramics, Ceram. Int. 34 (2008) 2067–2072, doi:10.1016/j.ceramint.2007.08.008.

[33] S.Y. Yoo, J.Y. Ha, S.J. Yoon, J.W. Choi, High-power properties of piezoelectric hard materials sintered at low temperature for multilayer ceramic actuators, J. Eur. Ceram. Soc. 33 (2013) 1769–1778, doi:10.1016/j.jeurceramsoc.2013.02.014.

[34] Y. Yan, K.H. Cho, S. Priya, Role of secondary phase in high power piezoelectric PMN-PZT ceramics, J. Am. Ceram. Soc. 94 (2011) 4138–4141, doi:10.1111/j.1551-2916.2011.04891.x.

[35] L. Wang, T.L. Zhao, X. Dai, J. Song, S. Dong, Conductive mechanism and the enhancement high-power electrical properties of Mn-modified Bi(Sc 3/4 In 1/4)O 3 –PbTiO 3 –Pb(Mg 1/3 Nb 2/3)O 3 high temperature piezoelectric ceramics, J. Mater. Sci. Mater. Electron. 30 (2019) 7780–7786, doi:10.1007/s10854-019-01093-7.

[36] D. Lin, K.W. Kwok, H.L.W. Chan, Piezoelectric and ferroelectric properties of KxNa1-xNbO3 lead-free ceramics with MnO2 and CuO doping, J. Alloys Compd. 461 (2008) 273–278, doi:10.1016/j.jallcom.2007.06.128.

[37] H. Takao, Y. Saito, Y. Aoki, K. Horibuchi, Microstructural evolution of crystalline-oriented (K0.5Na 0.5)NbO3 piezoelectric ceramics with a sintering aid of CuO, J. Am. Ceram. Soc. 89 (2006) 1951–1956, doi:10.1111/j.1551-2916.2006.01042.x.

[38] J. Wu, Y. Chang, B. Yang, S. Zhang, Y. Sun, F. Guo, W. Cao, Phase transitional behavior and electrical properties of Pb(In1/2Nb1/2)O3–Pb(Mg1/3Nb2/3)O3–PbTiO3 ternary ceramics, J. Mater. Sci. Mater. Electron. 26 (2015) 1874–1880, doi:10.1007/s10854-014-2623-6.

[39] S. Su, R. Zuo, D. Lv, J. Fu, Synthesis and characterization of (001) oriented BaTiO 3 platelets through a topochemical conversion, Powder Technol 217 (2012) 11–15, doi:10.1016/j.powtec.2011.09.045.

[40] H. Zhang, Y. Zhu, P. Fan, M.A. Marwat, W. Ma, K. Liu, H. Liu, B. Xie, K. Wang, J. Koruza, Temperature-insensitive electric-field-induced strain and enhanced piezoelectric properties of <001>textured (K,Na)NbO3-based lead-free piezoceramics, Acta Mater 156 (2018) 389–398, doi:10.1016/j.actamat.2018.07.005.

[41] F.K. Lotgering, Topotactical reactions with ferrimagnetic oxides having hexagonal crystal structures-II, J. Inorg. Nucl. Chem. 16 (1960) 100–108, doi:10.1016/0022-1902(60)80092-9.

[42] Y. Chang, Y. Sun, J. Wu, X. Wang, S. Zhang, B. Yang, G.L. Messing, W. Cao, Formation mechanism of highly [0 0 1]c textured Pb(In1/2Nb1/2)O3-Pb(Mg1/3Nb2/3)O3-PbTiO3 relaxor ferroelectric ceramics with giant piezoelectricity, J. Eur. Ceram. Soc. 36 (2016) 1973–1981, doi:10.1016/j.jeurceramsoc.2016.02.030.

[43] P.W. Rehrig, G.L. Messing, S. Trolier-McKinstry, Templated grain growth of barium titanate single crystals, IEEE Trans. Ultrason. Ferroelectr. Freq. Control. 47 (2000) 895–902, doi:10.1111/j.1151-2916.2000.tb01610.x.

[44] S. Zhang, F. Li, High performance ferroelectric relaxor-PbTiO 3 single crystals: Status and perspective, J. Appl. Phys. 111 (2012), doi:10.1063/1.3679521.

[45] S. Wada, H. Kakemoto, T. Tsurumi, Enhanced Piezoelectric Properties of Piezoelectric Single Crystals by Domain Engineering, Mater. Trans. 45 (2004) 178–187, doi:10.2320/matertrans.45.178.

[46] D. Damjanovic, Contributions to the piezoelectric effect in ferroelectric single crystals and ceramics, J. Am. Ceram. Soc. 88 (2005) 2663–2676, doi:10.1111/j.1551-2916.2005.00671.x.

[47] F. Li, D. Lin, Z. Chen, Z. Cheng, J. Wang, C. Li, Z. Xu, Q. Huang, X. Liao, L.Q. Chen, T.R. Shrout, S. Zhang, Ultrahigh piezoelectricity in ferroelectric ceramics by design, Nat. Mater. 17 (2018) 349–354, doi:10.1038/s41563-018-0034-4.

[48] N. Luo, S. Zhang, Q. Li, Q. Yan, W. He, Y. Zhang, T.R. Shrout, PMN-PT based quaternary piezoceramics with enhanced piezoelectricity and temperature stability, Appl. Phys. Lett. 104 (2014), doi:10.1063/1.4875797.

[49] Z. Liu, A.R. Paterson, H. Wu, P. Gao, W. Ren, Z. Ye, Synthesis, structure and piezo-/ferroelectric properties of a novel bismuth-containing ternary complex perovskite solid solution, J. Mater. Chem. C. 5 (2017) 3916–3923, doi:10.1039/c7tc00571g.

[50] J. Fu, R. Zuo, Z. Xu, High piezoelectric activity in (Na,K)NbO 3 based lead-free piezoelectric ceramics: Contribution of nanodomains, Appl. Phys. Lett. 99 (2011) 3–6, doi:10.1063/1.3624704.

[51] Y.M. Jin, Y.U. Wang, A.G. Khachaturyan, J.F. Li, D. Viehland, Adaptive ferroelectric states in systems with low domain wall energy: Tetragonal microdomains, J. Appl. Phys. 94 (2003) 3629–3640, doi:10.1063/1.1599632.

[52] Q. Liu, Y. Zhang, J. Gao, Z. Zhou, H. Wang, K. Wang, X. Zhang, L. Li, J.F. Li, High-performance lead-free piezoelectrics with local structural heterogeneity, Energy Environ. Sci. 11 (2018) 3531–3539, doi:10.1039/c8ee02758g.

[53] D.I. Woodward, J. Knudsen, I.M. Reaney, Review of crystal and domain structures in the PbZrxTi1-xO3 solid solution, Phys. Rev. B - Condens. Matter Mater. Phys. 72 (2005), doi:10.1103/PhysRevB.72.104110.

[54] R. Theissmann, L.A. Schmitt, J. Kling, R. Schierholz, K.A. Schönau, H. Fuess, M. Knapp, H. Kungl, M.J. Hoffmann, Nanodomains in morphotropic lead zirconate titanate ceramics: On the origin of the strong piezoelectric effect, J. Appl. Phys. 102 (2007) 1–6, doi:10.1063/1.2753569.

[55] Y. Sun, Y. Chang, J. Wu, Y. Liu, L. Jin, S. Zhang, B. Yang, W. Cao, Ultrahigh energy harvesting properties in textured lead-free piezoelectric composites, J. Mater. Chem. A. 7 (2019) 3603–3611, doi:10.1039/c8ta10312g.

[56] G.A. Rossetti, A.G. Khachaturyan, G. Akcay, Y. Ni, Ferroelectric solid solutions with morphotropic boundaries: Vanishing polarization anisotropy, adaptive, polar glass, and two-phase states, J. Appl. Phys. (2008) 103, doi:10.1063/1.2930883.

[57] G. Arlt, Twinning in ferroelectric and ferroelastic ceramics: stress relief, J. Mater. Sci. 25 (1990) 2655–2666, doi:10.1007/BF00584864.

[58] L. Luo, D. Zhou, Y. Tang, Y. Jia, H. Xu, H. Luo, Effects of Mn doping on dielectric and piezoelectric properties of 0.71Pb (Mg1/3Nb2/3)O3-0.29PbTiO3 single crystals, Appl. Phys. Lett. 90 (2007) 1–4, doi:10.1063/1.2711533.

[59] G. Du, R. Liang, L. Wang, K. Li, W. Zhang, G. Wang, X. Dong, Linear temperature scaling of ferroelectric hysteresis in Mn-doped Pb(Mn1/3Sb2/3)O3-Pb(Zr,Ti)O3 ceramic with internal bias field, Appl. Phys. Lett. 102 (2013) 0–4, doi:10.1063/1.4795442.

[60] Y. Li, J. Yuan, D. Wang, D. Zhang, H. Jin, M. Cao, Effects of Nb, Mn doping on the structure, piezoelectric, and dielectric properties of 0.8 Pb (Sn 0.46 Ti 0.54) O 3-0.2 Pb (Mg 1/3 Nb 2/3) O 3 piezoelectric ceramics, J. Am. Ceram. Soc. 96 (2013) 3440–3447, doi:10.1111/jace.12479.

[61] W.L. Warren, D. Dimos, G.E. Pike, K. Vanheusden, R. Ramesh, Alignment of defect dipoles in polycrystalline ferroelectrics, Appl. Phys. Lett. 67 (1995) 1689, doi:10.1063/1.115058.

[62] R. Lohkämper, H. Neumann, G. Arlt, Internal bias in acceptor-doped BaTiO3 ceramics: Numerical evaluation of increase and decrease, J. Appl. Phys. 68 (1990) 4220–4224, doi:10.1063/1.346212.

[63] X. Ren, Large electric-field-induced strain in ferroelectric crystals by point-defect-mediated reversible domain switching, Nat. Mater. 3 (2004) 91–94, doi:10.1038/nmat1051.

[64] Y. Gao, K. Uchino, D. Viehland, Time dependence of the mechanical quality factor in “hard” lead zirconate titanate ceramics: development of an internal dipolar field and high power origin, Jpn. J. Appl. Phys. 45 (2006) 9119–9124, doi:10.1143/JJAP.45.9119.

[65] J.C. Woolley, Introduction to solid state physics (1957), doi:10.1016/0022-5096(57)90051-0.

[66] N. Luo, S. Zhang, Q. Li, Q. Yan, Y. Zhang, T. Ansell, J. Luo, T.R. Shrout, Crystallographic dependence of internal bias in domain engineered Mn-doped relaxor-PbTiO3 single crystals, J. Mater. Chem. C. 4 (2016) 4568–4576, doi:10.1039/c6tc00875e.

[67] X. Qi, E. Sun, W. Lü, S. Li, B. Yang, R. Zhang, W. Cao, Dynamic characteristics of defect dipoles in Mn-doped 0.24Pb(In 1/2 Nb 1/2)O 3 -0.47Pb(Mg 1/3 Nb 2/3)O 3 -0.29PbTiO 3 single crystal, CrystEngComm 21 (2019) 348–355, doi:10.1039/c8ce01913d.

[68] X. shuang Qiao, X. ming Chen, H. li Lian, J. ping Zhou, P. Liu, Dielectric, ferroelectric, piezoelectric properties and impedance analysis of nonstoichiometric (Bi0.5Na0.5)0.94+xBa0.06TiO3 ceramics, J. Eur. Ceram. Soc. 36 (2016) 3995–4001, doi:10.1016/j.jeurceramsoc.2016.06.032.

[69] P. Li, B. Liu, B. Shen, J. Zhai, Y. Zhang, F. Li, X. Liu, Mechanism of significantly enhanced piezoelectric performance and stability in textured potassium-sodium niobate piezoelectric ceramics, J. Eur. Ceram. Soc. 38 (2018) 75–83, doi:10.1016/j.jeurceramsoc.2017.07.017.

[70] S. Zhang, N.P. Sherlock, R.J. Meyer, T.R. Shrout, Crystallographic dependence of loss in domain engineered relaxor-PT single crystals, Appl. Phys. Lett. 94 (2009) 108–111, doi:10.1063/1.3125431.